Journal of Molecular Liquids 384 (2023) 122199

Contents lists available at ScienceDirect

Journal of Molecular Liquids

journal homepage: www.elsevier.com/locate/molliq

On the solvation structures formed in conditioning-free MMAC-based electrolytes: A theoretical–experimental spectroscopic insight of interest to Mg battery area

Andrzej Eilmes [a,*], Wagner A. Alves [b,*]

[a] Faculty of Chemistry, Jagiellonian University, Gronostajowa 2, 30-387 Kraków, Poland
[b] Núcleo de Espectroscopia e Estrutura Molecular (NEEM), Departamento de Química, Instituto de Ciências Exatas, Universidade Federal de Juiz de Fora, 36036-900 Juiz de Fora-MG, Brazil

ARTICLE INFO

Keywords:
Experimental spectra
AIMD-simulated spectra
MMAC
THF
Diglyme

ABSTRACT

The 2.39:1 Mg:$MgCl_2$:$AlCl_3$ (MMAC)-tetrahydrofuran (THF) and 1:1.22 MMAC-diethylene glycol dimethyl ether (G2) electrolytes, which have been already investigated by electrochemical measurements, are studied in the current work by using experimental vibrational spectroscopy allied to ab initio molecular dynamics (AIMD) simulations of spectra. Raman data are practically identical to the 2:1 $MgCl_2$:$AlCl_3$ (MACC)-THF and 3:5 MACC-G2 binary systems, except for a 330 cm^{-1} band, commonly assigned to $[AlCl_3(THF)_{1,2}]$ and/or $[AlCl_2]^+$, which is absent for the THF-based ternary system. Subtle changes are also seen in the far-IR spectra, where a band at around 315 cm^{-1} shows strong dependence on the $MgCl_2$ content and so may be associated to the $[Mg_2(\mu\text{-}Cl)_3]^+$ dimer. The monomeric species, $[MgCl]^+$, is also observed in both electrolytes by means of IR bands at 270–285, 300 and 325–330 cm^{-1}. The varied amounts of monomer and dimer seem to be related to the electrochemical activities determined for these ternary systems.

1. Introduction

Magnesium aluminum chloride complex (MACC)-ether electrolytes are unexpensive, easily synthesized and have exhibited the best electrochemical performance among several all-inorganic salts studied so far [1]. However, the need for electrolytic conditioning to get good reversibility and mostly the poor temporal stability do limit the use of these electrolytes in practical battery systems [2]. At this point, it is worth stressing the increasing efforts of researchers in this area, not only due to the widespread success of electric vehicles, which work with lithium-ion battery packs, but also because the price of lithium will skyrocket since it has become an increasingly scarce resource [3].

Conditioning-free methods have been proposed in the literature aiming at improving Mg electrochemistry. One of them is based on the addition of Mg powder to the MACC-ether system, which is named MMAC and has provided unprecedent electrochemical performance results [4]. For instance, compared to 1:1 MACC-1,2 dimethoxyethane (DME), the overpotential of the MMAC-DME electrolyte was dropped from 354 to 164 mV and the Coulombic efficiency was increased from 85 to 92%. In the case of the MMAC-tetrahydrofuran (THF) electrolyte, 159 mV overpotential and 100% Coulombic efficiency were determined, in contrast to 2:1 MACC-THF, whose values were 400 mV and 72%. The MMAC-diethylene glycol dimethyl ether (G2) electrolyte exhibited 212 mV overpotential and 85% Coulombic efficiency, whereas values of 253 mV and 57% were obtained for the 1:2 MACC-G2 system. The introduction of Mg powder in the synthesis of the electrolytes caused changes in the Mg(II):Al(III) ratio, which was increased to 1.45:1, 2.39:1 and 1:1.22 in DME, THF and G2, respectively. Recently, the 1:1 MACC-DME and 1.45:1 MMAC-DME electrolytes have been also studied by vibrational spectroscopy and the solution data pointed out to the presence of $MgCl_2(DME)_2$, $[(\mu\text{-}Cl)_2Mg_2(DME)_4]^{2+}$ and $[(\mu\text{-}Cl)_4Mg_3(DME)_5]^{2+}$ [5,6]. The dimer, which was originally isolated and characterized by XRD measurements [7], is a highly electroactive species whereas the trimer could be correlated to the higher electrochemical performance exhibited in DME [4]. Nevertheless, such a relationship seems to be a controversial topic since this complex has not been identified by means of the interface Pourbaix diagram [8].

In a similar way to our recent study [6], it would be now advisable to spectroscopically investigate the MMAC-based electrolytes in the THF and G2 solvents aiming at evaluating whether higher Mg(II) complexes

* Corresponding authors.
E-mail addresses: eilmes@chemia.uj.edu.pl (A. Eilmes), wagner.alves@ufjf.br (W.A. Alves).

https://doi.org/10.1016/j.molliq.2023.122199
Received 16 March 2023; Received in revised form 16 May 2023; Accepted 24 May 2023
Available online 29 May 2023

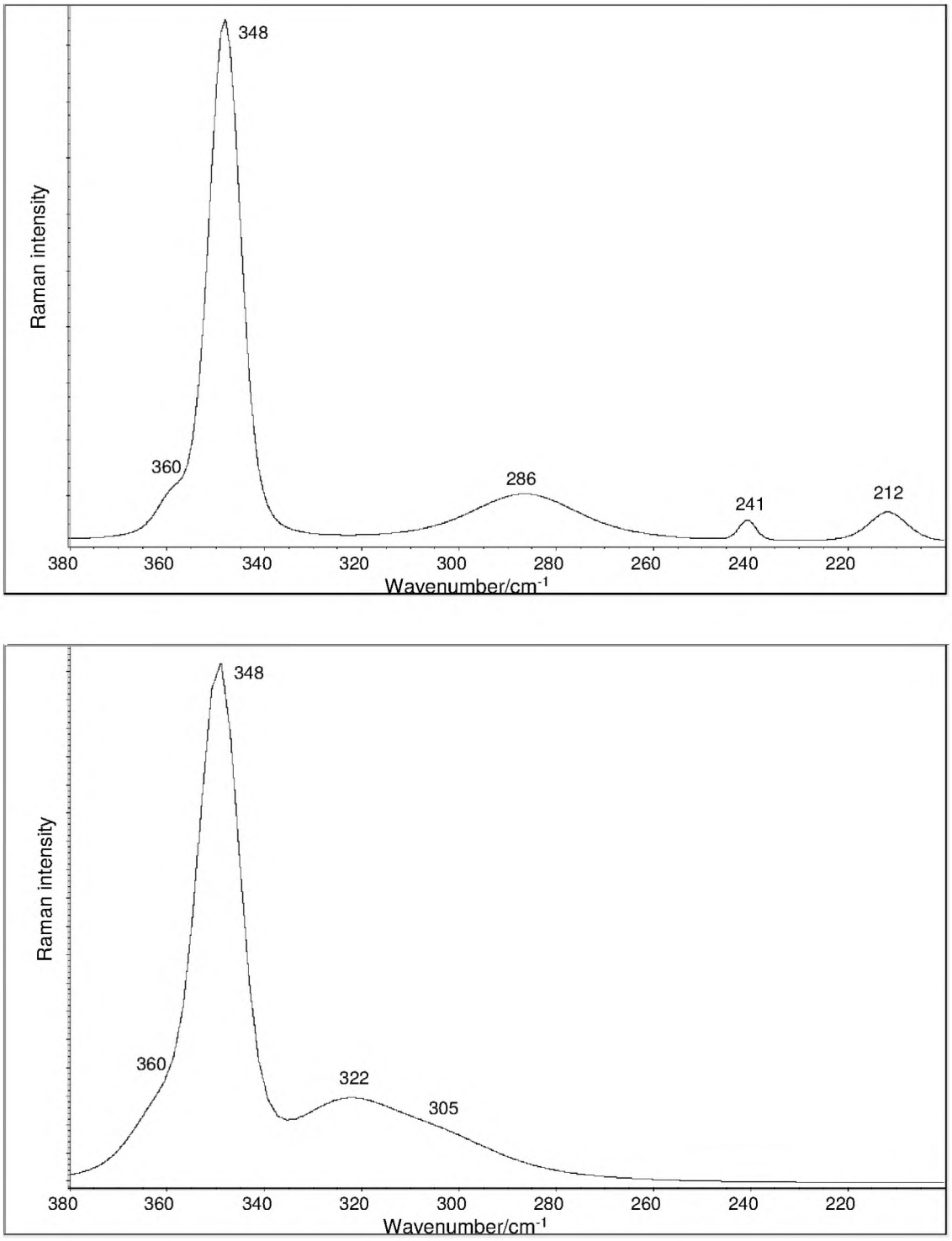

Fig. 1. Raman spectra of MMAC-based electrolytes: 2.39:1 in THF (top); 1:1.22 in G2 (bottom).

could be formed and identified by IR and Raman spectroscopies or $[(\mu\text{-Cl})_3Mg_2(THF)_6]^+$ and $[MgCl(G2)_2]^+$ would be preserved even at higher stoichiometries. Such a proposal stems from the fact that the former complex is the major electroactive species at the 2:1 MACC-THF electrolyte, but lowered amounts of this dimer are suggested for the 1:1 ratio [9,10], in which $[MgCl(THF)_5]^+$ stands out in accordance with the equilibrium (1):

$$MgCl_2 + [MgCl]^+ = [Mg_2(\mu - Cl)_3]^+ \quad (1)$$

On the other hand, the dimer was not identified in the concentration-dependent spectra of the 1:2 and 3:5 MACC-G2 electrolytes and such a fact suggests that the G2 coordinating power, or in other words the increase of the chelating effect may make hard the formation of dimers, trimers and so on [11]. We have noticed through the literature that the dimer is usually identified in solution by a Raman band at around 240 cm^{-1}. It is really intriguing how other Raman- and/or IR-active vibrational modes have not been yet reported for such a complex, mainly because it was already isolated by some authors [12,13].

In this work, the 2.39:1 MMAC-THF and 1:1.22 MMAC-G2 electrolytes are investigated by Raman and IR spectroscopies for the first time,

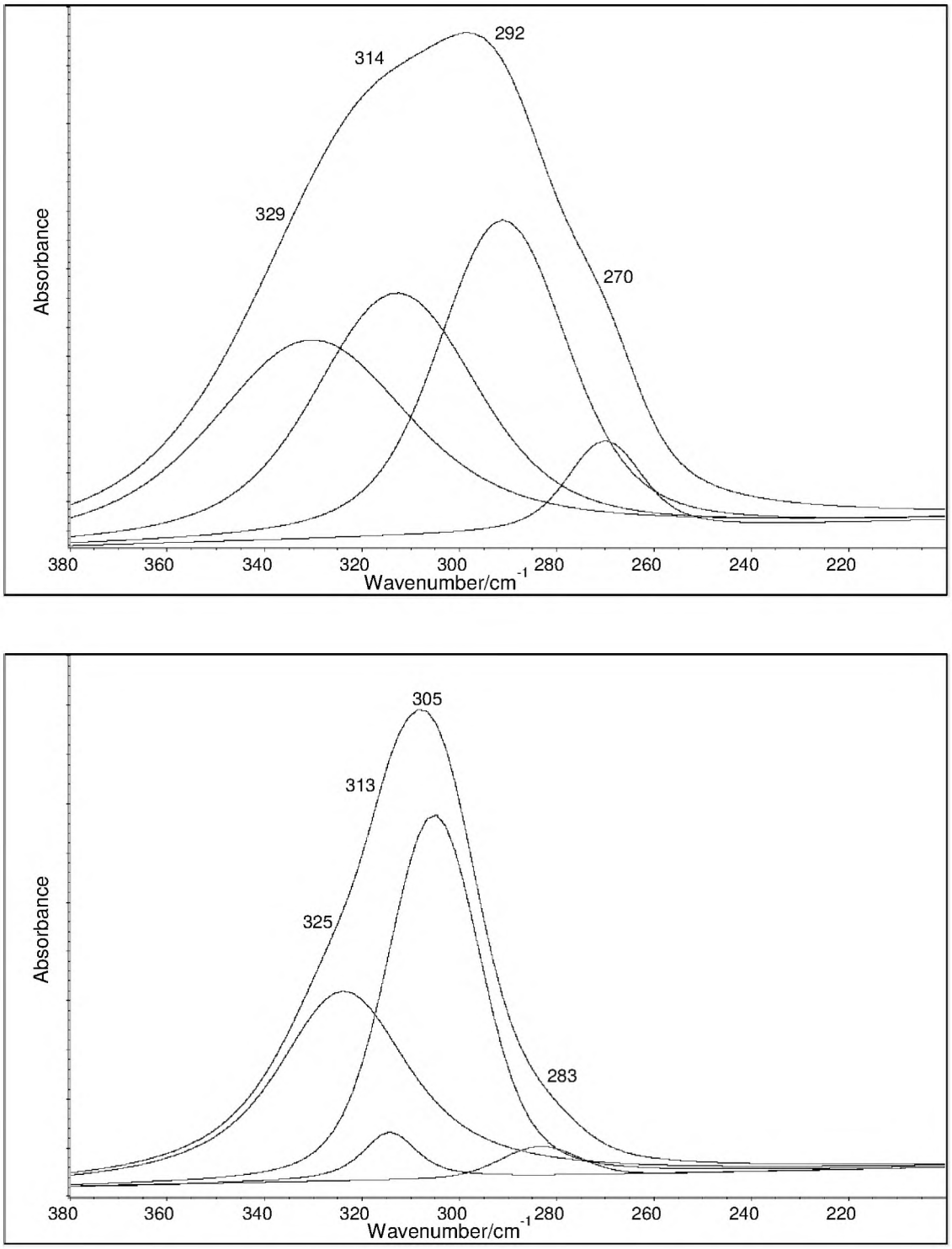

Fig. 2. Far-IR spectra of MMAC-based electrolytes: 2.39:1 in THF (top); 1:1.22 in G2 (bottom).

and undoubtedly, the motivation for the choice of these systems is very well justified by the aforementioned information. The experimental data are supplemented by ab initio molecular dynamics (AIMD) simulations of the vibrational spectra for relevant explicitly solvated ion aggregates. The MD methodology allows the system to cross the barriers between local energy minima and explore the energy surface, providing therefore a more realistic description of dynamically changing structures in the solvent. Our simulation protocol earlier used [6,10,11] now includes the $[AlCl_4]^-$ ion in order to account for the effects of interactions with the counterion and better spectroscopically describe the aggregates formed at those media.

2. Methodology

2.1. Experimental details

Tetrahydrofuran (≥99.9%), anhydrous diethylene glycol dimethyl ether (99.5%), magnesium powder (99.8%), magnesium dichloride (99.99%) and aluminum trichloride (99.99%) were purchased from Sigma-Aldrich. The solvents were dried over 3 Å molecular sieves prior

to use and chemicals were handled in a controlled N_2 atmosphere dry box. Reagent concentrations were higher than the ones employed in the work originally performed by Luo and coworkers [4]. Such a procedure was needed due to too low Raman scattering cross section of the bands assigned to ν_{MgCl} and ν_{MgO} vibrations. Regarding that the kinetics of the Mg deposition and stripping processes are greatly enhanced by increasing electrolyte concentration [14], our approach seems to be reliable. Similarly to our recent investigation [6], Mg powder was added after complete dissolution of the metal chlorides in the solvents, followed by stirring at 25 °C for 2 h (in THF) and 1 h (in G2). Excess Mg powder and other insoluble species were removed by filtration and the 2.39:1 MMAC-THF and 1:1.22 MMAC-G2 electrolytes exhibited clear aspect. Final Mg(II) and Al(III) molar concentrations were determined from inductively coupled plasma mass spectrometry (ICP-MS), being reported here only the content referring to the former cation (0.4 mol L^{-1} in both solvents).

Raman spectra were recorded on a Bruker SENTERRA dispersive Raman microscope, equipped with a thermoelectrically-cooled CCD detector and a long working-length objective (20x lens). The 785 nm line of a diode laser was used as Raman excitation source with power equal to 100 mW and the acquisition time for each spectrum was 60 s per window. IR spectra were acquired on a Nicolet FT-IR Magna 760 spectrometer using CsI windows. Both spectra were obtained with 4 cm^{-1} resolution at the temperature of 25 ± 2 °C.

OMNIC 7.3 software was used for spectra normalization and the curve-fitting analyses were very well supported by the second derivatives of the original spectra with respect to the number of components. During the fitting each one was considered to be a Voigt function, which provided the best results.

2.2. Computational details

AIMD simulations of Born-Oppenheimer MD were performed using GPU-accelerated Terachem v. 1.93 [15], running on Nvidia Tesla K40d GPUs. PBE functional was used with the 6–31 + G* basis set; the size of the basis set was limited to reduce the computational cost. The $MgCl_2$, $[MgCl]^+$ and $[Mg_2(\mu\text{-}Cl)_3]^+$ species with few explicit solvent molecules and the $[AlCl_4]^-$ counterion were embedded in implicit solvent modeled using the COSMO approach. The static dielectric constant of the continuous solvent was set to 7.4 and 7.426 for G2 and THF, respectively.

Initial simulations were performed at T = 298 K controlled via the Langevin thermostat. The structures were equilibrated during 10 ps of simulations with a time step of 1 fs. Then the NT simulations continued for another 40 ps. Next, five independent MD simulations in the NE ensemble were spawned from different points of the recorded NT trajectory and conducted for 20 ps with a time step of 0.5 fs. The total dipole moment of the system was calculated for each frame of the NE trajectories.

IR spectra of the systems were calculated from the AIMD simulations as Fourier transforms (FTs) of the autocorrelation function of the dipole moment and averaged over all five NE simulations for a given system type in order to account for changes in the spectra resulting from differences in the structure of complexes (different positions of the $[AlCl_4]^-$ counterion) and possible excitation of different modes in the NE part of simulations. To obtain the Raman spectra, the polarizability tensor was calculated for every second frame of the NE trajectory (i.e. a time step of 1 fs) and the spectrum was computed as the FT of the autocorrelation function of the polarizability. This procedure was computationally expensive and therefore it was applied to only one of the NE trajectories for a given system. Nevertheless, the averaging is of lesser importance if the Raman spectra are well resolved in the range of interest. Finally, FTs of selected geometrical parameters (interatomic distances or angles) were calculated to assess information on possible local oscillations which may contribute to the global vibrational modes in the spectra.

3. Results and discussion

Fig. 1 (top) illustrates the Raman spectrum of the 2.39:1 MMAC-THF electrolyte in the range 380–200 cm^{-1}. The 212 cm^{-1} band (ν_{MgCl}) is very well established in the literature and belongs to $MgCl_2(THF)_4$, which has been also observed at the 2:1 ratio [9], but it is absent for the 1:1 stoichiometry [10]. Although such a precursor can be seen in the spectrum, its fraction involved in the Lewis acid-base reaction gives rise to $[(\mu\text{-}Cl)_3Mg_2(THF)_6]^+$ and $[AlCl_4]^-$, which are characterized by the respective bands at 241 (ν_{MgCl}) and 348 cm^{-1} (ν_{AlCl}) [16,17]. This latter is always much more intense than the ones usually attributed to the Mg complexes, as also confirmed by the shoulder at around 360 cm^{-1}, which is assigned to the ν_{MgO} mode [18]. The 286 cm^{-1} band is well known and corresponds to the THF ring pucker vibration [19]. Additionally, the absence of the 328 cm^{-1} band (ν_{AlCl}), which is due to $[AlCl_3THF]$ and/or $[AlCl_2(THF)_2]]^+$, suggests full conversion to $[AlCl_4]^-$ and this is a very important step to prevent a latent Al cementation reaction and so Mg corrosion [20,21]. In Fig. 1 (bottom) the Raman spectrum of the 1:1.22 MMAC-G2 electrolyte shows a band envelope with maxima at 322 and 305 cm^{-1} corresponding to distinct conformers of liquid G2 [22]. Again, the band characteristic of $[AlCl_4]^-$ comes along with a shoulder and both are observed at the same aforementioned wavenumbers. Although an acid-base reaction has already taken place at the medium, no band can be observed at the region characterized by the ν_{MgCl} vibrations. Regarding that the current Raman spectra are identical to the ones obtained for the 2:1 MACC-THF [9] and 3:5 MACC-G2 [11] electrolytes, one can realize that the $[(\mu\text{-}Cl)_3Mg_2(THF)_6]^+$ and $[MgCl(G2)_2]^+$ complexes seem to govern the ternary systems too. About the latter complex, the high ionic character of the Mg-Cl bond is responsible for the absence of a Raman band associated to this vibration, which is IR-active and has been already reported by our research group [10,11]. Hence, we shall use the far-IR technique not only to supplement Raman data, but also to unravel the puzzling about the vibrations of $[Mg_2(\mu\text{-}Cl)_3]^+$.

Far-IR spectra of the 2.39:1 MMAC-THF and 1:1.22 MMAC-G2 electrolytes are depicted in Fig. 2 for the same spectral range. As already shown in our previous works [10,11], the solvents do not interfere at the studied region and so the interpretation for the observed trend is facilitated. The number of components under the band envelope is the same in both systems, but one clearly observes that the half-height width is significantly reduced in going from top to bottom due to the intensity decrease of the component at around 315 cm^{-1}. Note that such behavior is in line with the one observed in the Raman spectra (Fig. 1), in which the band of the dimer at 241 cm^{-1} cannot be seen for the G2-based ternary system. This trend allows us to assign this feature to the ν_{MgO} vibration of $[(\mu\text{-}Cl)_3Mg_2(THF)_6]^+$ and its position is in agreement with the one reported for the $[Mg(H_2O)_6]^{2+}$ complex [18]. The band at 270–285 cm^{-1} and the most intense signal near 300 cm^{-1} have been already reported for lower stoichiometries and correspond to ν_{MgCl} strongly coupled to ν_{MgO} of $[MgCl(THF)_5]^+$ and $[MgCl(G2)_2]^+$ [10,11]. The IR analysis of these ternary systems was useful to reconsider us assignments made on the higher wavenumber side, where a band at around 330 cm^{-1} can be still observed. It has been assigned to the ν_{AlCl} vibration activated by the entry of one or two THF molecules into Al(III) coordination sphere. However, the Raman spectrum of the THF-based ternary system indicates that the Lewis acid was totally converted to the anion and unreacted $MgCl_2(THF)_4$ is also identified. Hence, we believe that such a band may be attributed to the ν_{MgO} mode of the monomer, which is present in both systems. The greater amount of this species could be then related to the lower electrochemical activity of the 1:1.22 MMAC-G2 electrolyte. In other words, the strong attraction between Mg(II) and one chlorine atom as well as the high G2 chelating power makes hard the delivery of the cation onto the electrode. The IR data are also in excellent accordance with mass spectrometry results, in which both monomer and dimer were detected in G2, being the former the predominant species [21].

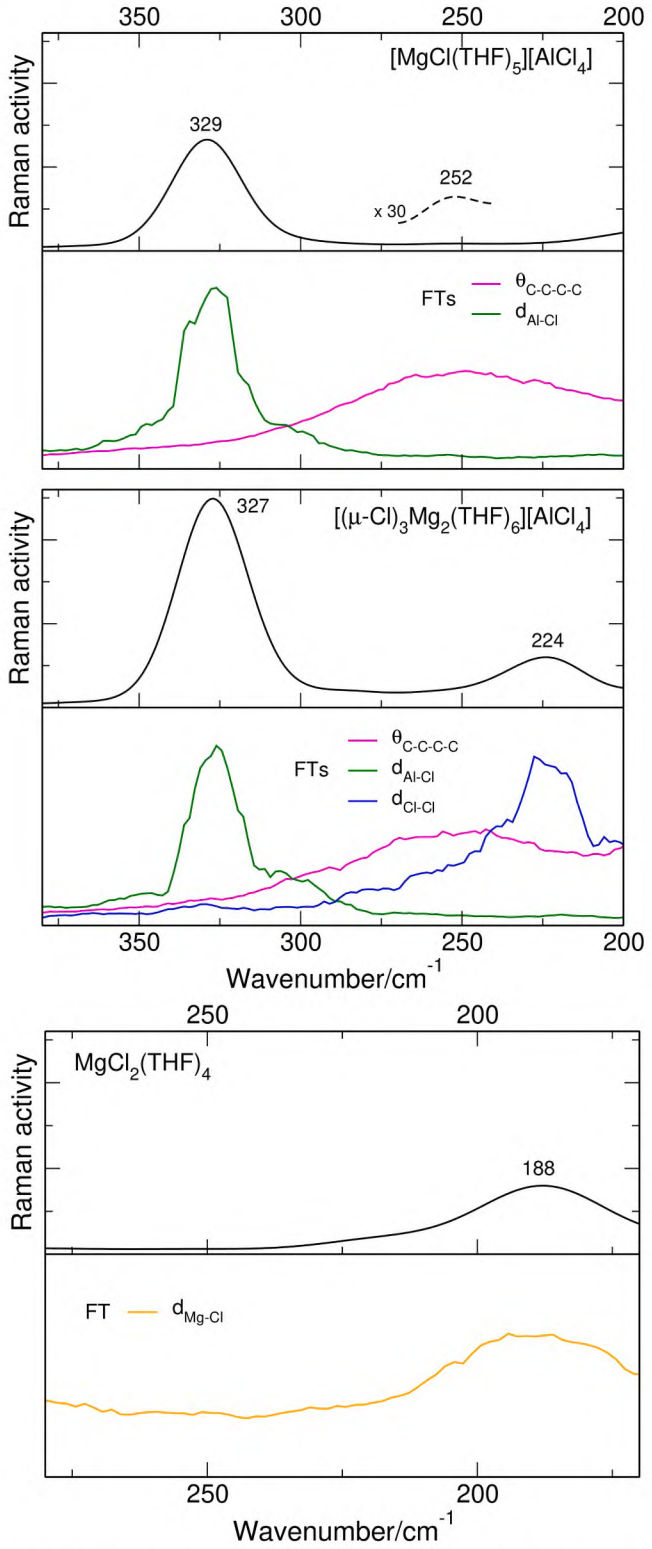

Fig. 3. Simulated Raman spectra of $[MgCl(THF)_5][AlCl_4]$ (top), $[(\mu\text{-}Cl)_3Mg_2(THF)_6][AlCl_4]$ (middle) and $MgCl_2(THF)_4$ (bottom). FTs of selected parameters are shown in lower parts of each panel.

The Raman spectra simulated for $[MgCl(THF)_5][AlCl_4]$, $[(\mu\text{-}Cl)_3Mg_2(THF)_6][AlCl_4]$ and $MgCl_2(THF)_4$ are shown in Fig. 3 along with the FTs of selected geometrical parameters. For the former, the peak at 329 cm^{-1} undoubtedly corresponds to the stretching vibration of the $[AlCl_4]^-$ anion, as corroborated by the FT of the Al-Cl distances. No appreciable signal is seen at lower wavenumbers, so confirming the high

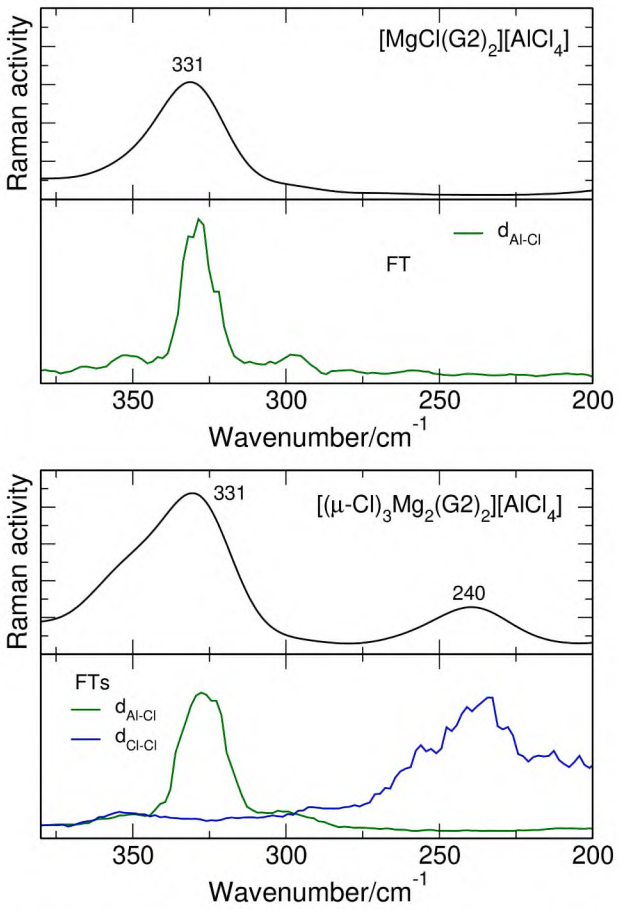

Fig. 4. Simulated Raman spectra of $[MgCl(G2)_2][AlCl_4]$ (top) and $[(\mu\text{-}Cl)_3Mg_2(G2)_2][AlCl_4]$ (bottom) with FTs for Al-Cl and Cl-Cl distances.

polarization in the Mg-Cl bond. On the other hand, a barely noticeable maximum may be observed at 252 cm^{-1} and its position is in line with the FT of the dihedral angle formed by the four carbon atoms of the THF ring. We believe this weak signal may be then assigned to the ring-puckering vibration of this solvent, even though only few THF molecules were employed in the system, resulting in a too small solvent-to-salt ratio to yield proper estimate of its intensity. Similar conclusion is reached for the second aggregate, in which the FT of the THF dihedral angle suggests a poor feature at around 250 cm^{-1}, but it is now hidden under a 224 cm^{-1} band, which is due to the oscillations of the Cl-Cl-Cl triangle in the μ-bridged core. Again, the most intense band at 327 cm^{-1} is attributed to the ν_{AlCl} mode of $[AlCl_4]^-$. Concerning the $MgCl_2(THF)_4$ complex, the FT for the Mg-Cl distance clearly shows that the Raman-active mode calculated at 188 cm^{-1} corresponds to the stretching vibration involving such an oscillator. One can observe that the calculated wavenumbers are systematically shifted to lower energies compared to experimental data and this effect can be attributed to the deficiencies in the description of the interactions with the solvent within the basis set/functional combination used in our AIMD simulations. Despite this, the theoretical data do confirm that $MgCl_2(THF)_4$, $[(\mu\text{-}Cl)_3Mg_2(THF)_6]^+$ and $[AlCl_4]^-$ are detectable species by Raman spectroscopy, in contrast to the $[MgCl(THF)_5]^+$ complex.

The simulated Raman spectra of $[MgCl(G2)_2][AlCl_4]$ and $[(\mu\text{-}Cl)_3Mg_2(G2)_2][AlCl_4]$ in the range 380–200 cm^{-1} are dominated by the 331 cm^{-1} band readily assigned to the ν_{AlCl} vibration of the anion (Fig. 4). As expected, additional bands are not observed in the calculated spectrum of $[MgCl(G2)_2][AlCl_4]$, in contrast to the $[(\mu\text{-}Cl)_3Mg_2(G2)_2][AlCl_4]$ aggregate, which exhibits a distinct band at 240 cm^{-1} corresponding to the vibrations of the $[Mg_2(\mu\text{-}Cl)_3]^+$ core, as indicated by the

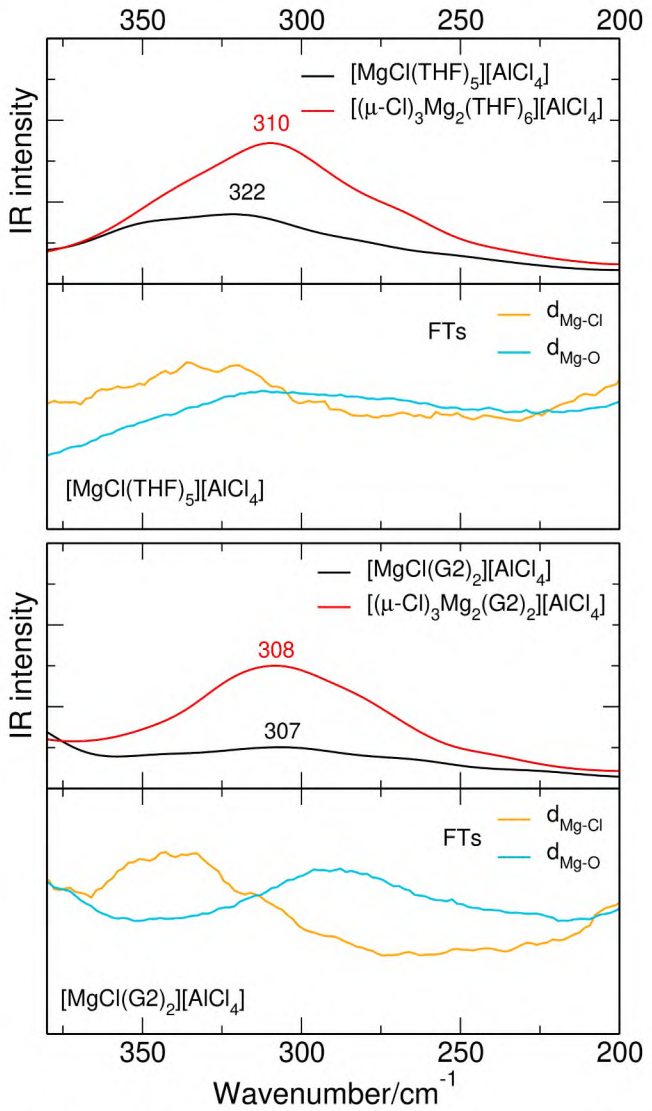

Fig. 5. Simulated IR spectra of $MgCl^+$ and $[Mg_2(\mu\text{-}Cl)_3]^+$ aggregates with solvent molecules: THF (top) and G2 (bottom).

FT of the Cl-Cl distances. These findings confirm the conclusions drawn from the experimental spectrum (Fig. 1 (bottom)), in which detectable dimer amounts are not produced in the 1:1.22 MMAC-G2 electrolyte.

Simulated IR spectra of $[MgCl]^+$ and $[Mg_2(\mu\text{-}Cl)_3]^+$ in the presence of the counterion and THF and G2 molecules are shown in Fig. 5. One observes that the ν_{MgCl} and ν_{MgO} vibrations are, indeed, strongly coupled and contribute to the modes at about 300 cm^{-1}, as clearly indicated by sample FTs of Mg-Cl and Mg-O distances. The IR spectra averaged over 5 MD trajectories are broad and no individual bands can be clearly distinguished under the envelope. Nevertheless, the intensity of the band related to the $[Mg_2(\mu\text{-}Cl)_3]^+$ complex is always higher than the one of the signal associated to the $[MgCl]^+$ cation, and the ratio of the dimer-to-monomer IR absorption cross-sections is remarkably greater in G2. Note this trend differs from the experimental result (Fig. 2) and, therefore, allows us to assure that tiny dimer amounts are formed at the 1:1.22 MMAC-G2 electrolyte, but they are increased at the 2.39:1 MMAC-THF system.

4. Conclusions

Measurements of the IR and Raman spectra were combined with AIMD-simulated vibrational spectra to elucidate the solvates formed at the 2.39:1 MMAC-THF and 1:1.22 MMAC-G2 electrolytes, which have exhibited unprecedent electrochemical performance [4]. Trimers and/or higher Mg(II) aggregates were not detected in the current work, unlike a theoretical study in which the $[Mg_3(\mu\text{-}Cl)_5]^+$ species was predicted as the most stable multinuclear aggregate in G2, even though the stoichiometry dependence has not been deemed [23]. Here, the vibrational spectra of the ternary systems are close to the ones recently reported for THF- and G2-based binary systems [9,11], but varied quantities of $[MgCl]^+$ and $[Mg_2(\mu\text{-}Cl)_3]^+$ were identified from the far-IR spectra and supported by simulations in the presence of the counterion. The IR band envelope with maximum at around 300 cm^{-1} has the half-height width substantially reduced in going from the 2.39:1 MMAC-THF to the 1:1.22 MMAC-G2 electrolyte and such a change is due to the intensity decrease of the band at around 315 cm^{-1}, which is assigned to the dimer and reported for the first time in the literature. Although the tridentate nature of G2 makes difficult the formation of higher Mg(II) aggregates, the small quantities of the dimer are related to the significant change of the 1:2 ratio [11] to the 1:1.22 stoichiometry, poorly shifting the equilibrium (1) to the right side. The reduced amounts of the dimeric species are responsible for the lower electrochemical activity of the G2-based ternary electrolyte as compared to the THF-based one. Finally, the higher electrochemical performance of the ternary systems in relation to the binary ones seems to be due to the lower $AlCl_3$ content, which is deemed a deleterious species [20,21].

CRediT authorship contribution statement

Andrzej Eilmes: Writing – original draft, Writing – review & editing.
Wagner A. Alves: Writing – original draft, Writing – review & editing.

Declaration of Competing Interest

The authors declare that they have no known competing financial interests or personal relationships that could have appeared to influence the work reported in this paper.

Data availability

Data will be made available on request.

Acknowledgments

This study was financed by the Fundação de Amparo à Pesquisa do Estado de Minas Gerais/FAPEMIG, Coordenação de Aperfeiçoamento de Pessoal de Nível Superior/CAPES and Financiadora de Estudos e Projetos/FINEP. AE gratefully acknowledges Poland's high-performance computing infrastructure PLGrid (HPC Center ACK Cyfronet AGH) for providing computer facilities and support within computational grant no. PLG/2022/015595.

References

[1] C.J. Barile, R.G. Nuzzo, A.A. Gewirth, Exploring salt and solvent effects in chloride-based electrolytes for magnesium electrodeposition and dissolution, J. Phys. Chem. C 119 (24) (2015) 13524–13534.
[2] Y. Li, S. Guan, H. Huo, Y. Ma, Y. Gao, P. Zuo, G. Yin, A review of magnesium aluminum chloride complex electrolytes for Mg batteries, Adv. Funct. Mater. 31 (2021) 2100650.
[3] R. Shah, V. Mittal, E. Matsil, A. Rosenkranz, Magnesium-ion batteries for electric vehicles: Current trends and future perspectives, Adv. Mechan. Eng. 13 (2021) 1–9.
[4] J. Luo, S. He, T.L. Liu, Tertiary Mg/$MgCl_2$/$AlCl_3$ inorganic Mg^{2+} electrolytes with unpreceddent electrochemical performance for reversible Mg deposition, ACS Energy Lett. 2 (2017) 1197–1202.
[5] V.O. Chaffin, M.C. Pessanha, W.A. Alves, Solvation structures formed in the $MgCl_2$:$AlCl_3$-dimethoxyethane system: a look through Raman and IR spectroscopies, Vib. Spectrosc. 100 (2019) 167–171.
[6] A. Eilmes, W.A. Alves, Theory-experiment partnership applied to the spectroscopic analysis of a promising conditioning-free electrolyte for Mg batteries, J. Mol. Liq. 350 (2022), 118528.

[7] Y. Cheng, R.M. Stolley, K.S. Han, Y. Shao, B.W. Arey, N.M. Washton, K.T. Mueller, M.L. Helm, V.L. Sprenkle, J. Liu, G. Li, Li, Highly active electrolytes for rechargeable Mg batteries based on a $[Mg_2(\mu\text{-}Cl)_2]^{2+}$ cation complex in dimethoxyethane, Phys. Chem. Chem. Phys. 17 (20) (2015) 13307–13314.
[8] A. Kopač Lautar, J. Bitenc, R. Dominko, J.-S. Filhol, Building ab initio interface Pourbaix diagrams to investigate electrolyte stability in the electrochemical double layer: application to magnesium batteries, ACS Appl. Mater. Interfaces 13 (7) (2021) 8263–8273.
[9] V.O. Chaffin, W.A. Alves, Composition dependence on the spectral behavior of magnesium aluminum chloride complex electrolytes, J. Mol. Liq. 315 (2020), 113722.
[10] A. Eilmes, W.A. Alves, Combining experimental and theoretical vibrational spectroscopy to study magnesium aluminum chloride complex electrolytes, J. Mol. Liq. 333 (2021), 116053.
[11] A. Eilmes, W.A. Alves, Unraveling the solvates in a diethylene glycol dimethyl ether-based electrolyte: A computational-experimental spectroscopic contribution to Mg battery area, J. Mol. Liq. 359 (2022), 119251.
[12] H.S. Kim, T.S. Arthur, G.D. Allred, J. Zajicek, J.G. Newman, A.E. Rodnyansky, A. G. Oliver, W.C. Boggess, J. Muldoon, Structure and compatibility of a magnesium electrolyte with a sulphur cathode, Nat. Commun. 2 (2011) 427.
[13] Z. Zhao-Karger, X. Zhao, O. Fuhr, M. Fichtner, Bisamide based non-nucleophilic electrolytes for rechargeable magnesium batteries, RSC Adv. 3 (2013) 16330–16335.
[14] K.A. See, Y.-M. Liu, Y. Ha, C.J. Barile, A.A. Gewirth, Effect of concentration on the electrochemistry and speciation of the magnesium aluminum chloride complex electrolyte solution, ACS Appl. Mater. Interfaces 9 (41) (2017) 35729–35739.
[15] Terachem v. 1.93; http://www.petachem.com/.
[16] N. Pour, Y. Gofer, D.T. Major, D. Aurbach, Structural analysis of electrolyte solutions for rechargeable Mg batteries by stereoscopic means and DFT calculations, J. Am. Chem. Soc. 133 (16) (2011) 6270–6278.
[17] Y. Vestfried, O. Chusid, Y. Goffer, P. Aped, D. Aurbach, Structural analysis of electrolyte solutions comprising magnesium-aluminate chloro-organic complexes by Raman spectroscopy, Organometallics 26 (13) (2007) 3130–3137.
[18] W.W. Rudolph, G. Irmer, G.T. Hefter, Raman spectroscopic investigation of speciation in $MgSO_4$(aq), Phys. Chem. Chem. Phys. 5 (2003) 5253–5261.
[19] B. Cadioli, E. Gallinella, C. Coulombeau, H. Jobic, G. Berthier, Geometric structure and vibrational spectrum of tetrahydrofuran, J. Phys. Chem. 97 (30) (1993) 7844–7856.
[20] G. Bieker, M. Salama, M. Kolek, Y. Gofer, P. Bieker, D. Aurbach, M. Winter, The power of stoichiometry: conditioning and speciation of $MgCl_2/AlCl_3$ in tetraethylene glycol dimethyl ether-based electrolytes, ACS Appl. Mater. Interfaces 11 (2019) 24057–24066.
[21] L.C. Merrill, J.L. Schaefer, Electrochemical properties and speciation in Mg $(HMDS)_2$-based electrolytes for magnesium batteries as a function of ethereal solvent type and temperature, Langmuir 33 (37) (2017) 9426–9433.
[22] P. Johansson, J. Grondin, J.-C. Lassègues, Structural and vibrational properties of diglyme and longer glymes, J. Phys. Chem. A 114 (39) (2010) 10700–10705.
[23] P. Jankowski, J.M.G. Lastra, T. Vegge, Structure of magnesium chloride complexes in ethereal systems: computational comparison of THF and glymes as solvents for magnesium battery electrolytes, Batteries Supercaps. 3 (2020) 1350–1359.